Article:
Alborzi, E. orcid.org/0000-0002-2585-0824, Yong, X., Roostaeinia, M. orcid.org/0000-0002-6101-3230 et al. (4 more authors) (2024) Effect of zeolite 3.7˚A coated monoliths on improvement of aviation fuel thermal oxidative stability. Fuel, 360. 130498. ISSN: 0016-2361

https://doi.org/10.1016/j.fuel.2023.130498

Fuel 360 (2024) 130498

Contents lists available at ScienceDirect

Fuel

journal homepage: www.elsevier.com/locate/fuel

Full Length Article

Effect of Zeolite 3.7 Å coated monoliths on improvement of aviation fuel thermal oxidative stability

Ehsan Alborzi [a,*], Xue Yong [b], Morteza Roostaeinia [c], Detlev C. Mielczarek [d], Irina S. Flyagina [e], Simon G. Blakey [f], Mohamed Pourkashanian [a]

[a] Department of Mechanical Engineering, The University of Sheffield, Sheffield, S3 7RD, UK
[b] Department of Chemistry, The University of Sheffield, Sheffield, S3 7HF, UK
[c] Physics Department, Virginia Tech (Virginia Polytechnic Institute and State University), USA
[d] Independent Contributor, Ile-de-France, France
[e] A.N. Frumkin Institute of Physical Chemistry and Electrochemistry, Russian Academy of Sciences, 31, bld.4, Leninsky Prospect, Moscow, 119071, Russia
[f] Department of Mechanical Engineering, The University of Birmingham, Birmingham, B15 2TT, UK

ARTICLE INFO

Keywords:
Aviation Fuel
Thermal stability
Zeolite
Fuel treatment
Adsorption
Molecular modeling

ABSTRACT

The effect of zeolite 3.7 Å acidity on the reduction of surface deposition propensity of a Jet A-1 fuel, with marginal thermal oxidative stability was studied. This was achieved through treatment of the fuel in a packed bed reactor, using three types of monolithic zeolite with different Si/Al ratios. It was found that the increase of acidity is directly proportional to the surface deposition reduction such that the treatment with the highest ratio (Si/Al = 25) resulted in the most significant surface propensity reduction. However, a combination of zeolite with the lowest acidity (Si/Al = 17) and the activated carbon exhibited the greatest improvement of thermal oxidative stability. As a general trend, for all three Si/Al ratios in the monolithic zeolites used in this work, surface deposition propensity of the Jet A-1 fuel decreased markedly with the increase of monolithic size. Nevertheless, it is anticipated that efficacy will reach an steady state after a certain point. Quantum chemistry calculations demonstrate that polar species can interact with the CHA and 2Al doped chabazite in a number of ways, from dispersion interactions to forming covalent and hydrogen bonds. Furthermore, our calculations suggest that the doping CHA with Al enhanced the adsorption of polar species, which agree with a lab-scale experiment with the model fuel.

1. Introduction

Thermal oxidative degradation of aviation fuels is an important characteristic observed in modern gas turbine propulsion engines. Oxidative degradation occurs prior to the combustion chamber, where the fuel is used as a heat sink to cool down the turbo machinery lubricants. It is commonly known that under such conditions, when aviation fuel is exposed to a thermal load, a series of free radical reactions occur in the bulk fuel. When the bulk fuel temperature is in the range of 100 °C to 300 °C, the free radical reactions are categorized as auto-oxidative, initiating from reactions between dissolved O_2 and alkyl radicals [1]. The auto oxidation reactions result in the formation of a number of soluble and insoluble complex organic macro-molecules, composed of hydrocarbons, sulfur, nitrogen and oxygen [2–10]. These molecules eventually partake in the formation of carbonaceous deposits on the wetted surfaces of fuel system components. Such deposits have a negative impact on the functionality of jet fuel system components; they obstruct filter screens, fuel nozzles, disrupting the flow of fuel, and ultimately compromise the performance of engine hardware.

It is known that deoxygenation may result in a reduction of the surface deposition propensity of a fuel. The net effect of fuel deoxygenation on surface deposition propensity is attributed to hindering the formation of peroxy radicals, at early stages of autoxidation [9–12]. Two well-known practical methods of fuel deoxygenation are nitrogen purging and membrane separation [13]. However, the effectiveness of these methods largely depends on the concentration of polar species in jet fuels, including traces of phenolic molecules, reactive sulfur species, nitrogen-containing molecules, dissolved metals and oxygenated hydrocarbon species.

We previously reported that for a Jet A-1 fuel type with a marginal thermal oxidative stability, the extent of the surface deposition reduction, that is achieved through the removal of heteroatomic species, is considerably more significant than with fuel deoxygenation [14,15].

* Corresponding author.
E-mail address: e.alborzi@sheffield.ac.uk (E. Alborzi).

https://doi.org/10.1016/j.fuel.2023.130498
Received 8 March 2023; Received in revised form 15 November 2023; Accepted 25 November 2023
Available online 8 December 2023

These findings are supported by experimental results, showing that very pure fuels, e.g., synthetic sustainable aviation fuels with an extremely low content of heteroatomic species, produce very low levels of deposits, even when the fuels are fully saturated with air. The higher sensitivity of the thermal oxidative stability of aviation fuels to the presence of polar species, compared to dissolved O_2, is a key point for practical applications, given that at relatively higher altitude, typical of cruise and start of descent conditions, the availability of O_2 is already limited.

Adsorbents such as attapulgite clay and activated carbon efficiently reduce the surface deposition propensity of aviation fuels by removing different types of polar species present in the fuel [15]. Zeolite with pore size 3.7 Å (also know as chabazite (CHA)), has been shown to be a strongly selective adsorbent for a number of heteroatomic species [14], as well as a weaker adsorbent for dissolved molecular oxygen, according to lab-scale studies [14,16].

The crystalline structure of zeolites with a network of cavities and pores permits preferential adsorption of molecules that are smaller than the zeolite's pore diameter [17–19]. Different types of interactions between species and zeolites are reported including: Van der Waals forces between zeolite pore walls and adsorbate molecules and electrostatic interactions between adsorbate molecules and Brönsted acid sites of the zeolite [19]. A third interaction not discussed further in this work is adsorbate–adsorbate interactions [19]. In the case of aviation fuel treatment, quantum chemistry calculations suggest that two types of interaction between the species and adsorbent dominate. Dissolved molecular oxygen is removed by chabazite via physisorption, while the underlying process of oxygenated species removal by chabazite is predominantly of a chemical nature involving H-migration [20].

Zeolites are further characterized by their aluminium content, which determines their acidity, playing a crucial role in the determination of the adsorption selectivity of the sorbent [21]. This parameter is typically described by the Si/Al ratio, which can vary over a wide range. As the Si/Al ratio increases, the number of acid sites decreases. However, their strength of acidity can increase [22–24]. Furthermore, variations in the Si/Al ratio within different kinds of zeolite species result in variations of the zeolite, such as the amount and distribution of negative charge density in the structural frameworks and pores [25–28].

In this work, we investigate and assess: (i) the impact of different ratios of Si/Al on the reduction of the surface deposition propensity for a Jet A-1 fuel type, and (ii) study the performance of a combined bed, composed of activated carbon and zeolite 3.7 Å with Al/Si ratio = 17, on the reduction of surface deposition propensity. We used monolithic reactors as they are a preferential alternative to a conventional pelletized packed bed reactor, due to the comparatively lower pressure-drop and larger surface area. Monoliths, such as those utilized in this study, consist of a ceramic block, with a multitude of separated channels, coated with a thin layer of zeolites, which collectively form a honeycomb structure at the block cross-section, extruded along the tube reactor [29].

In the theoretical part of the study, ab-initio density functional theory calculations are used to elucidate molecular interactions between a number of aviation fuel representative polar species (aniline, BHT, dibutyldisulfide and Fe-naphthenate) with the zeolite. This work continues from the study of adsorption of oxygenate species from a Jet A-1 fuel type, by the same authors [20].

2. Computational details of the quantum chemistry simulations

The calculations were conducted using the CP2K/Quickstep package [30] with periodic boundary conditions (PBC) applied in the XYZ directions. These conditions followed the Generalized Poisson Solver (PSOLVER) framework for electrostatic calculations. The computational methodology employed geometry optimizations utilizing the Broyden–Fletcher–Goldfarb–Shanno (BFGS) algorithm [31], in conjunction with Density Functional Theory (DFT) computations.

Table 1
Composition of major hydrocarbon constituents along with sulfur, polar nitrogen-containing species, hydroperoxides and dissolved metals for the baseline fuels.

Compounds	Jet A-1 fuel	Polar-free solvent
n-Paraffins	20.67 % m/m	97.2 % m/m
iso-Paraffins	24.77 % m/m	NA
Cyclic hydrocarbons	30.84 % m/m	NA
Alkylbenzenes	16.18 % m/m	1.1 %
Indans and tetralins	2.15 % m/m	NA
Naphtalenes	1.33 % m/m	NA
Antioxidant	25 mg/l	NA
Acidity	0.08 mg KOH/100g	NA
Thiols, Sulfides and Disulfides	835 mg/kg	NA
Polar Nitrogen Species	12 mg/kg	NA
Total hydroperoxides	34.3 µM	2.5 µM
Dissolved Fe	115 ppb	NA
Dissolved Cu	50 ppb	NA
Dissolved Zn	51 ppb	NA

The Perdew–Burke–Ernzerhof (PBE) exchange–correlation functional [32], coupled with Goedecker–Teter–Hutter (GTH) pseudopotentials [33], and supported by the MOLOPT double-ζ basis sets (DZVP-MOLOPT-SR-GTH) [34], was employed for the atomic constituents: oxygen (O), silicon (Si), aluminium (Al), potassium (K), carbon (C), and hydrogen (H). The expansion of the charge density using plane waves utilized an energy cut-off of 350 Ry, in addition to a relative cut-off of 50 Ry within the multigrid scheme.

For the self-consistent field (SCF) iterations, both inner and outer iterations were capped at 25 and 20 respectively, while maintaining a convergence threshold of 5.0 × 10-6. The applied preconditioning approach was FULL_ALL, and DIIS was implemented as the minimizer, ensuring a robust convergence of the electronic structure calculations.

3. Experimental work

3.1. Test fuel composition

Two baseline fuels are used in this work, namely a Jet A-1 fuel with marginal thermal oxidative stability, and a model fuel, i.e., a polar-free solvent, composed of five normal alkanes in the range of C_{10} to C_{14}. The chemical composition of major hydrocarbon constituents along with the key species related to deposit formation in the Jet A-1 fuel sample as well as the chemical compositions of the model fuel are shown in Table 1. The Jet A-1 fuel sample was analyzed externally for major hydrocarbon speciation, reactive sulfur-containing species, antioxidants, and polar nitrogen-containing species, employing a test method developed by Intertek UK. This method identifies sulfur-containing species as well as group types in middle distillates. It uses an Agilent 7890 N gas Chromatograph with Zoex thermal modulation and an Agilent 355 sulfur chemiluminescence detector. The individual hydrocarbon constituents of the fuel are identified according to "UOP Method 990-11". This method determines the molecular-type homologous series based on the number of carbon atoms. Quantitative analysis of sulfur classes is carried out via the normalization of the total sulfur content determined by combustion followed by UV-fluorescence. This analysis separates sulfur-containing species based on their boiling points and polarity. This allows for the separation of the benzothiophenes and dibenzothiophenes into two distinct bands, separated from thiophenes, sulfides, and mercaptans.

3.2. Experimental setup 1: Packed bed reactor

A series of small-scale experiments are carried out in a packed bed reactor to explore the improvement of fuel thermal oxidative stability from fuel treatment by monolithic blocks coated with chabazite 3.7 Å. The monolithic block is shown in Figs. 1a and 1b. Each monolithic

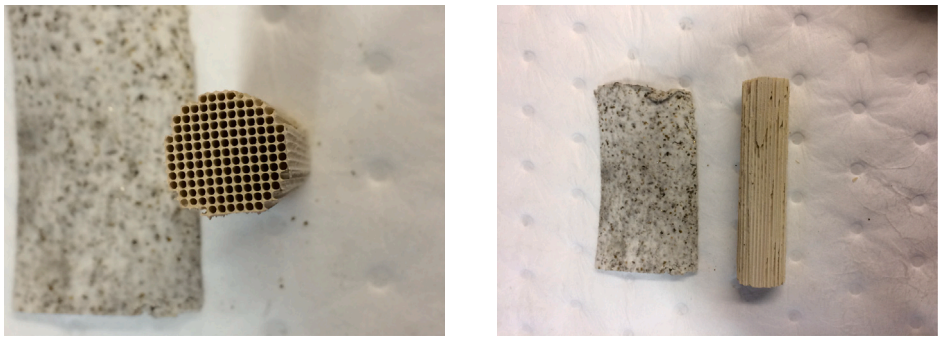

(a) cross-section (b) side view

Fig. 1. Cross-section and side view of the zeolite coated monolithic block.

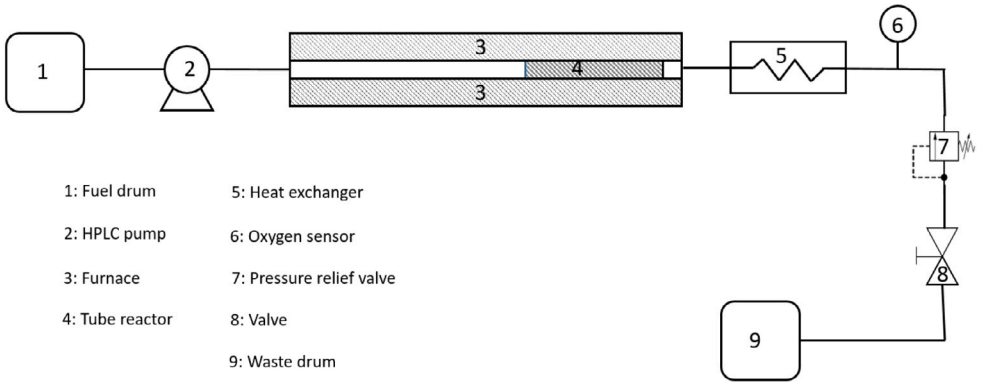

Fig. 2. Schematic of the fuel treatment test set up.

block is 7.62 cm long with a specific surface area of 300 m^2/g to 400 m^2/g and a density of 2.1 g/cm^3. Two parameters are considered for adsorptive treatment: the length of the packed bed corresponding to the number of monolithic blocks, and zeolite acidity corresponding to the ratio of Si/Al in chabazite (e.g., 17, 22, 25). An additional experiment was carried out to examine the performance of a combined bed, composed of equal lengths of activated carbon and monolithic chabazite, on the fuel thermal oxidative stability improvement. Each test was run on a fresh new monolithic block of chabazite.

As shown in Fig. 2, the packed bed reactor consists of a 1 m stainless steel tube with a 2.54 cm inner diameter, placed in the centerline of a temperature controlled furnace. 6 K-type thermocouples are brazed at equidistant intervals of 15 cm to the exterior of the stainless steel tube. The thermocouples permit thermal monitoring to ensure that the bed temperature remains constant throughout the tests. A proportional integral derivative (PID) controller is used to control and maintain the heating of the furnace, up to a fixed set point temperature of around 70 °C, prior to each test. Pressure is controlled via a pressure relieve valve that was set to open slightly above atmospheric pressure. The amount of dissolved O_2 is measured in-line, using an optical oxygen sensor (manufactured by Metler Toledo) during each experiment, placed approximately 1 m downstream of the tube reactor. After each fuel treatment test, the impact of the process on the fuel is evaluated through a subsequent "High Reynolds Thermal Stability" (HiReTS) test on the treated sample. Given that a standard complete HiReTS test requires 5 L of jet fuel (including test volume and rinsing), the low flow rate in the packed bed reactor means that each test requires approximately 17 h to prepare a sufficient volume of treated fuel for subsequent HiReTS evaluation.

The experimental protocol applied in this work was elaborated in cooperation with the industrial partners (Rolls Royce and Johnson Matthey) during the development of the test apparatus. First, the reactor is prepared with the monolithic blocks under ambient conditions, filled with the test fuel and placed in the initially cold furnace. As the HPLC pump flow rate is low, it is important that the flow reactor itself is manually primed, i.e. filled, with the test fuel prior to connecting the pump. Next, the prepared reactor is connected to the HPLC pump that circulates fuel through the test apparatus, initially under ambient temperature to permit calibration of the oxygen sensor to a stable baseline value. Once the oxygen sensor readings have stabilized, the temperature of the reactor is gradually raised to the pre-defined set-point. Fuel that passes through the reactor during the preparation and preheating stages is directed to a waste drum. It is considered that the fuel treatment commences once the furnace reaches thermal equilibrium, so that fuel inside of the reactor rapidly reaches the target set-point temperature, reducing the effect of a gradual temperature rise on the air solubility in the fuel [35].

3.3. Experimental setup 2: HiReTS and fuel thermal stability

In the HiReTS testing method, an aerated test fuel is filtered and pumped through an electrically heated capillary under a turbulent or transient flow regime. The capillary-tube heating is controlled to maintain a constant fuel temperature of 290 °C at the tube outlet.

The external surface of the capillary is blackened to ensure high thermal emissivity. A pyrometer is used to measure the real-time changes in the capillary wall temperature with a high degree of accuracy in twelve pre-defined measurement positions. Over the course of a test, the formation of carbonaceous deposits on the inner surface of the capillary tube creates an insulating effect on the inside of the tube, reducing heat transfer to the fuel, leading to localized areas of elevated external wall temperatures along the capillary tube. Throughout the test, the automated positioning of the pyrometer allowed the creation of a time-dependent profile of the localized temperature along the capillary tube external walls. A quantitative measure, known as the HiReTS number, is employed to interpret the results obtained from

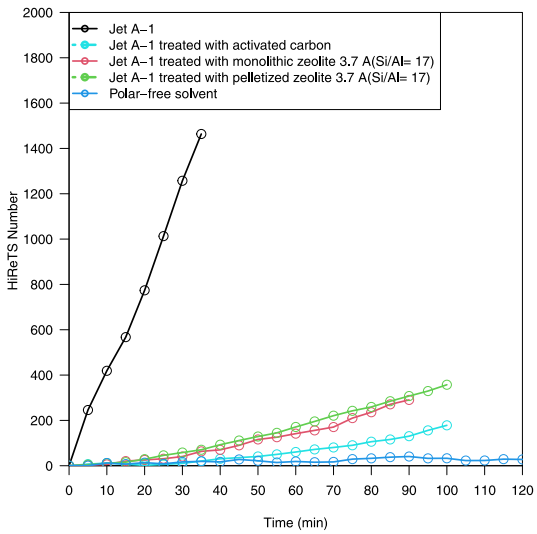

(a) Jet A-1 fuel, without and with zeolite treatment and polar-free solvent

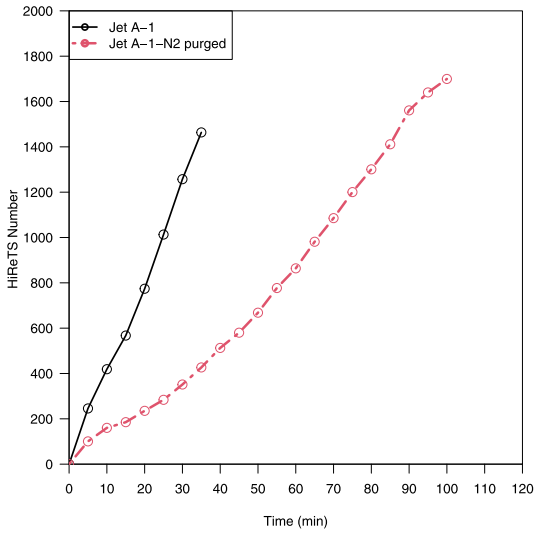

(b) Jet A-1 without and with deoxygenation (nitrogen purging)

Fig. 3. Surface deposition propensity results of pre and post treatment Jet A-1, polar-free solvent, pre and post deoxygenated Jet A-1.

Table 2
HiReTS test conditions.

Flow rate	35 ml/min
Exit temperature	290 °C
Test Pressure	2.0 MPa
Test Time	120 min
Number of measurement positions per scan	12
Scans per test	25
Distance between measurement positions	2.5 mm
Fuel aeration time	12 min
Scan time	5 min

the HiReTS test based on the evolution of the external capillary wall temperature during the test (ΔT). It is implied that the external wall temperature increases with deposits reducing the heat transfer between the fuel and capillary tube wall. Hence a higher HiReTS number corresponds to a larger amount, or a thicker layer of deposits within the capillary tube. The total HiReTS number is calculated by summing these temperature differences between the initial and final temperatures at each measurement position, as presented in Eq. (1):

$$HiReTS\ number = \sum_{n=1}^{n=12} (\Delta T_{Final,n} - \Delta T_{min,n}) \quad (1)$$

The standard test configuration as employed in the HiReTS is presented in Table 2.

To investigate the fundamental adsorption mechanisms of polar species using both the monolithic bed and the combined bed (activated carbon + monolithic bed), the polar-free solvent was doped with a predetermined quantity (200 ppm) of representative polar species commonly found in fuels. These selections were made with consideration of their functional groups and their roles in the thermal degradation of fuels. Following this preparation, the resulting solution underwent treatment using the beds as previously described. The quantification of the treated solution was accomplished through chromatographic analysis conducted before and after the treatment process. The polar species chosen for this investigation included butylated hydroxytoluene (BHT), Dibutyl Disulfide (DBDS), aniline, and Fe-naphthenate. While we acknowledge that the length and molecular weight of polar species in aviation fuel significantly surpass those of the polar species utilized in this study, the limited availability of appropriate options prompted us to proceed with the selected species.

4. Results and discussion

4.1. Effect of chabazite treatment on surface deposition propensity of Jet A-1 fuel with marginal thermal oxidative stability

Fig. 3(a) presents the effect of various types of treatment of the Jet A-1 fuel on the surface deposition propensity, as well as comparison with the two baseline fuels. Fig. 3(b) indicates the effect of deoxygenation, via N_2 purging, of the Jet A-1 fuel on the surface deposition propensity.

The results shown in Fig. 3(b) illustrate that the surface deposition propensity of a Jet A-1 with marginal thermal oxidative stability improved with nitrogen purging, however the overall performance of the fuel remains inadequate with a HiReTS number close to about 2000, which is too high. In contrast one can observe from Fig. 3(a) that the treatment of the same Jet A-1 fuel in the packed bed reactor with either pelletized or monolithic coated chabazite results in a substantial reduction in surface deposition propensity, illustrated by the much lower HiReTS number of around 400. In addition, Fig. 3(a) also illustrates that thermal stability can be further improved when the chabazite treatment is combined with an activated carbon stage, giving a HiReTS number of around 200. The polar-free solvent exhibits the highest thermal oxidative stability amongst all test cases due to the absence of heteroatomic species.

This behavior of fuel was previously reported [14], and is hypothesized to be linked to the initiation and propagation steps of the Basic Autoxidation of Scheme (BAS) for liquid hydrocarbons, as shown in Table 3, as reported in literature [6–11,36–38].

As the BAS indicates, at the initiation stage of the autoxidation cycle (rxn1), alkyl radicals (R·) are generated via a surface catalyzed slow reaction, which is not yet well understood. The R· radicals react rapidly with dissolved O_2 through a barrierless reaction (rxn3), forming peroxy radicals(RO_2·). Subsequently, RO_2· can attack the bulk species (RH), and abstract one atom of H, forming a hydroperoxide species(ROOH) and a R· radical (rxn4). A further initiation reaction is pertinent to the thermal decomposition of hydroperoxides (rxn2). Given that aviation Jet fuel contains micromolar level of these species, thermal decomposition of hydroperoxides is a viable reaction to initiate the cycle.

In the case of near-complete deoxygenation of the marginal Jet A-1 fuel, formation of RO_2· via rxn3 is interrupted. In such a condition,

Table 3
The most important classes of species and reaction families participating in BAS. The unit of activation energy is in kcal/mol and the unit of pre exponential factor for uni molecular and bi molecular reactions are s^{-1} and $L\,mol^{-1}s^{-1}$.

	Basic Autoxidation Scheme for Liquid Hydrocarbons	optimized values A	E_a
1	Initiator ⟶ R·	5.4E13	68.0
2	RO_2H ⟶ RO· + OH·	5.2E13	33.0
3	R· + O_2 ⟶ RO_2·	8.5E10	0
4	RO_2· + RH ⟶ RO_2H + R·	5.7E10	14.8
5	RO_2H + RO_2H ⟶ RO· + RO_2· + H_2O	3.2E9	24.1
6	OH· + RH ⟶ H_2O + R·	2.6E9	5.0
7	RO· + RH ⟶ ROH + R·	1.8E9	5.2
8	RO· ⟶ Rprime· + $R{=}O_{ketone}$	2.8E12	9.0
9	Rprime· + RH ⟶ alkane + R·	1E10	10.1
10	RO· + RO· ⟶ ROH + $R{=}O_{aldehyde}$	1.5E9	17.5
11	RO· + RO_2· ⟶ RO_2H + $R{=}O_{ketone}$	3.1E11	10.2
12	RO_2· + RO_2· ⟶ ROOOR	9.6E10	0
13	ROOOR ⟶ RO· + RO· + O_2	2.8E13	0.9
14	RO· + R· ⟶ RH + $R{=}O_{ketone}$	2.1E9	7.5
15	RO· + R· ⟶ RH + $R{=}O_{aldehyde}$	3.4E9	9.8
16	RO· + RO· ⟶ ROOR	2.7E9	0
17	RO· + R· ⟶ ROR	2.7E9	0
18	R· + R· ⟶ R_2	2.6E10	0
19	RO_2· ⟶ R· + O_2	1.1E16	19.0

if the concentration of ROOH is relatively high, the probability of self-reaction of these species (rxn5) becomes higher [12,14,39]. Given that the activation energy of rxn5 is approximately 6 kcal mol^{-1} lower than rxn2, formation of RO_2· can still take place under deoxygenated conditions through the pathway of rxn5. It is noteworthy that RO_2· partakes in the formation of insoluble chemical species via reaction with the radicals of phenolic antioxidants.

Previous work suggests that the remarkable improvement in surface deposition propensity of a Jet A-1 fuel with marginal thermal oxidative stability, after treatment with chabazite, is attributed to the substantial removal of dissolved metals, polar nitrogen-containing species, phenolic antioxidants, and oxygenated species. Collectively, these species play a strong role in the formation of insoluble agglomerated materials, leading to the carbonaceous surface deposition [14]. Treatment of aviation fuel with activated carbon results in the partial removal of the reactive sulfurs [15]; a class of species that also exhibits a strong effect on the surface deposition.

4.2. Effect of Si/Al ratio and monolith length on surface deposition propensity

As shown in Fig. 4, as a general trend, for all three Si/Al ratios in monolithic zeolites used in this work, surface deposition propensity of Jet A-1 decreased markedly with an increase in monolith length. This is evidenced by a sharp drop in the HiReTS number. Nevertheless, the reduction of surface deposition propensity became less noticeable with the increase of the monolith length, and it is anticipated that it would have reached an steady state after a certain length.

It is shown that the positive impact of aviation fuel treatment with zeolite 3.7 Å, on surface deposition reduction, is directly proportional to the Si/Al ratio such that the treatment with the highest ratio (Si/Al = 25) resulted in the most significant surface propensity reduction. We hypothesized that this is attributed to the increase of strength of acidity, which is associated with the decrease of Al content in zeolite. In theory, the change of Si/Al ratio in zeolite results in changes to the locations, the amount and the distribution of negative charge density in the structural frameworks which collectivity can intensify the molecular interactions between zeolite and polar heteroatomic species in jet fuel, which is shown in the following subsection.

It is further shown in Fig. 4 that the treatment of Jet A-1 fuel with the combined bed, composed of activated carbon and CHA with the lowest ratio (Si/Al = 17), had an almost identical impact as CHA with the highest ratio (Si/Al = 25) with respect to the reduction of surface deposition propensity.

In order to explain this behavior we focused on the adsorption of the polar species (added to the polar-free solvent), in the packed bed reactor experiments. Fig. 5(a) indicates that in the case of treatment with chabazite (Si/Al = 17) adsorption of BHT, Fe-naphthenate and oxygenated species began instantly, followed by a sudden adsorption rate increase before reaching a steady state phase. However, the maximum removal capacity of these species by chabazite is rather different. It appears that the adsorption of aniline began after a hold-off period of around 100 min, followed by a sharp increase over the next 300 min of the experiment, with a maximum removal capacity of approximately 65%, the same as Fe-naphthenate. A slightly longer hold-off period for the adsorption of DBDS is observed compared to aniline, however, the maximum removal capacity of dibutyldisulfide was lower than 5%. Fig. 5(b) presents the same behavior for the adsorption of the polar species by the combined bed of activated carbon and (Si/Al = 17). A substantial adsorption of DBDS was observed, which is attributed to the strong interaction between activated carbon and this species, which was previously reported [15].

4.3. Understanding of molecular interactions between chabazite and aviation fuel representative fuel species in adsorptive treatment

The chabazite (CHA) model was constructed using a crystallographic information file (cif) [40]. To investigate the effects of Al doping, we replaced two Si atoms in CHA with Al to form CHA-Al_2. Consequently, we positioned the two Al atoms within different large channels of CHA, maintaining an Al-Al distance of 13 Å. We introduced two potassium atoms to ensure charge compensation. All atomic positions in both CHA and CHA-Al_2 were relaxed prior to adding the adsorbents to the structures.

Moving forward, our investigation delved into the adsorption capabilities of various fuel components within the channels of CHA and CHA-Al_2. We conducted computations to explore the adsorption of aniline, BHT, DBDS, and Fe-naphthenate. Our analysis encompassed diverse approaches, where the adsorbate molecules approached the CHA surfaces from multiple angles, including perpendicular and parallel orientations binding to the surface through different atoms/functional groups. Additionally, we explored scenarios where the molecules penetrated through the pores. The choice of approach depended on the size and shape of the molecules.

Consequently, we identified configurations displaying the most negative energies, thus representing the most plausible adsorption modes. These configurations, characterized by the most negative energies,

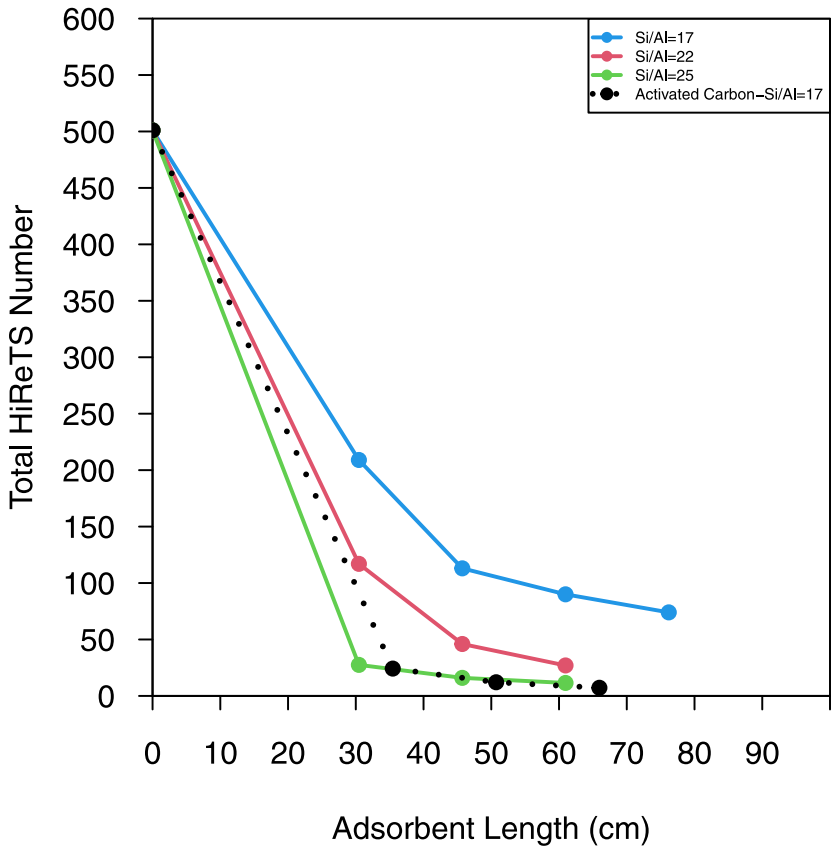

Fig. 4. Effect of Si/Al ratio on surface deposition propensity of the Jet A-1 fuel.

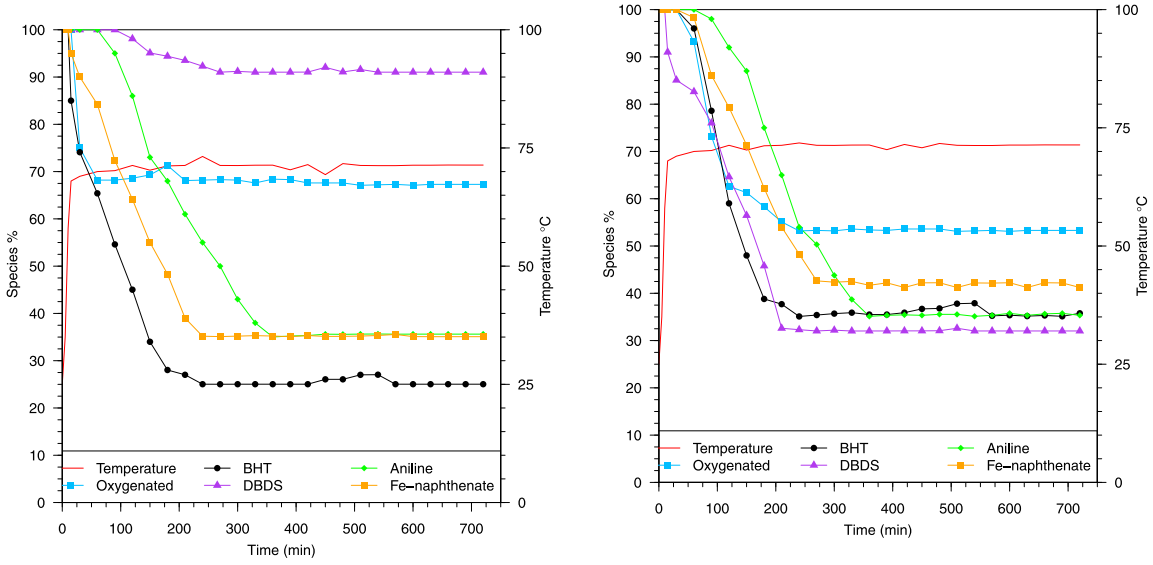

(a) Treatment with zeolite Si/Al= 17. Measurement errors for the polar species are ±5 %; and ±2 °C

(b) Treatment with combined bed(activated carbon and chabazite Si/Al= 17).Measurement errors for the polar species are ±5 %; and ±2 °C

Fig. 5. Comparative plot of fuel treated with zeolites as well as fuel treated with both zeolites and activated carbon.

were then selected as the most likely adsorption modes, and their corresponding adsorption energies were computed.

The corresponding adsorption energies are illustrated in (see Fig. 6).

All the adsorbents exhibited strong interactions with CHA, resulting in binding energies of −0.34 eV for BHT, −1.02 eV for Aniline, −1.33 eV for DBDS, and −0.93 eV for Fe-naphthenate. The stable adsorption mainly come from dispersion interactions to forming covalent and hydrogen bonds between the adsorbent and the pore surface. Following Al-doping, the adsorption interactions intensified. The adsorption energies experienced an increase ranging from 0.12 eV to 0.50 eV. These findings imply that Al replacement significantly enhances the selective adsorption of fuel components. Such an enhanced adsorption is attributed to the charge localization of HOMO orbitals. To explain this, in Fig. 7c–d, we present the plotted charge distribution of the HOMO

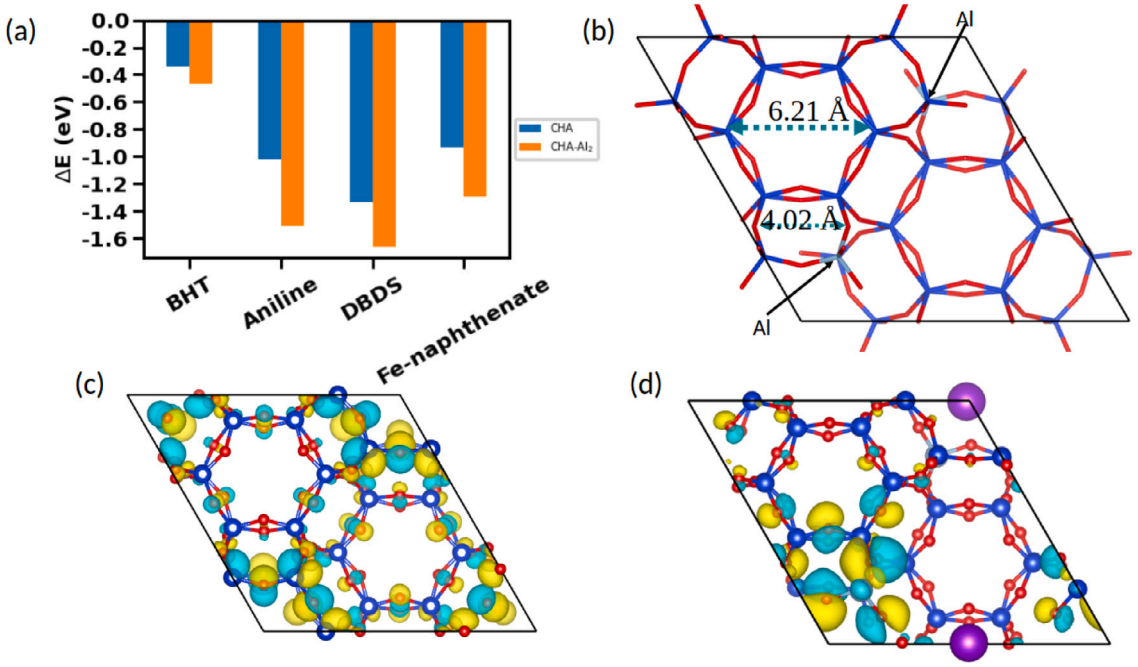

Fig. 6. (a) The adsorption energies of BHT, Aniline, DBDS, and Fe-naphthenate on CHA and CHA-Al2, (b) the general structure of CHA (c) and (d) the highest occupied molecular orbital of CHA and CHA-Al2. (red for O, and blue for Si, moss for Al). (For interpretation of the references to color in this figure legend, the reader is referred to the web version of this article.)

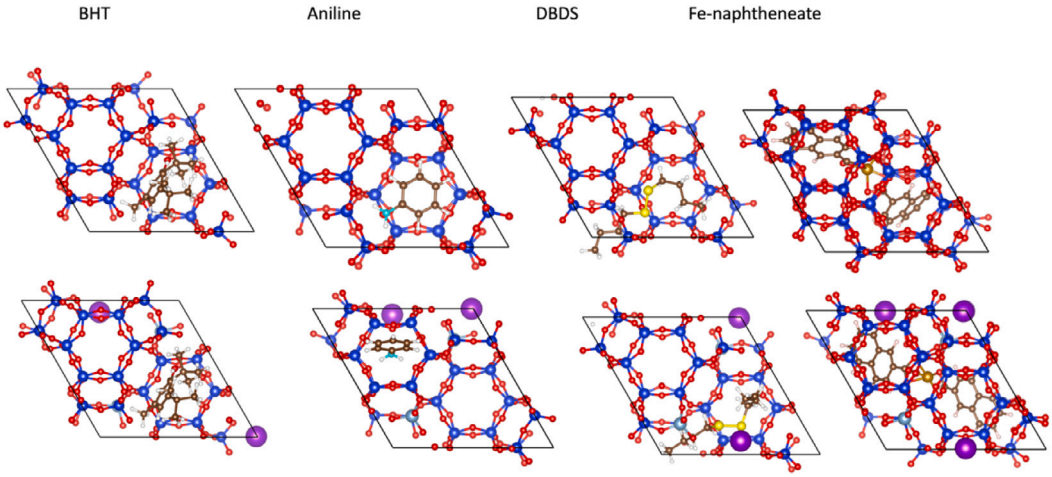

Fig. 7. The most stable adsorption configuration of BHT, Aniline, DBDS, and Fe-naphthenate on CHA and CHA-Al2. (red: O, blue: Si, purple: K, brown : C, white: H, yellow : sulfur, cyan : N, moss: Al). (For interpretation of the references to color in this figure legend, the reader is referred to the web version of this article.)

orbitals for CHA and CHA-Al_2 (see Fig. 6 c and d). The HOMO of CHA displays delocalization across the entire Si-O framework, whereas the HOMO of CHA-Al_2 exhibits localization. This localized charge distribution is anticipated to result in more potent electrostatic or Van der Waals interactions with the adsorbents.

All the structures of CHA/CHA-Al_2 with adsorbents are presented in Fig. 7. It is evident that the size of BHT is larger than that of the other adsorbents, leading to its capturing within the pores. With a relatively weaker adsorption (lower adsorption energies), BHT remained the least abundant species after passing through the zeolite. Aniline and Fe-naphthenate exhibited stronger binding to the channel due to their smaller sizes and the presence of Fe-O interactions, making them the second least abundant species. In the case of DBDS, although it exhibited stronger adsorption energies, it still persisted as the dominant species after passing through the zeolite. The possible reason for this might be that DBDS possesses a much smaller width (1.78 Å) than the pore size (4.02 Å or 6.21 Å). This discrepancy allows DBDS to more easily traverse the monolith channel without spending sufficient time interacting with the active surface of the zeolite. For a more comprehensive understanding of this particular scenario, further exploration through in-depth molecular dynamics simulations is necessary.

5. Conclusions

This publication presents an experimental and theoretical investigation aimed at further substantiating the influence of polar species on the stability of aviation fuel. We provide results from experimental studies that compare the behavior of dopants representing fuel compounds in a “model fuel”. Furthermore, we showcase the effectiveness of a treatment process using both the model fuel and real jet fuel in a small-scale test setup. It is important to note that upscaling for practical application was not within the scope of our study.

We demonstrate that, for Jet A-1 fuel with marginal thermal oxidative stability, the removal of polar species serves as a highly efficient means to enhance thermal stability. This removal was achieved through the utilization of solid adsorbents, such as zeolite with a pore size of 3.7 Å and activated carbon.

In the case of CHA-based adsorbents, the strength in acidity, as determined by the Si/Al ratio, was found to be directly proportional to the reduction in surface deposition. Treatment using the highest ratio (Si/Al = 25) resulted in the most pronounced reduction in surface deposit formation propensity. Generally, across the three Si/Al ratios in monolithic zeolites utilized in this study, the surface deposition propensity of Jet A-1 fuel decreased significantly with an increase in monolith size. However, this reduction in surface deposition propensity becomes less apparent with the increase in monolith length, and it is expected to stabilize after a certain length. A combination of zeolite with the lowest acidity (Si/Al = 17) and activated carbon yielded the most significant improvement in thermal oxidative stability.

Ab initio quantum chemistry calculations are employed to elucidate the observed results. These calculations illustrate that polar species can interact with both CHA and the 2Al-doped chabazite cluster through various mechanisms, including dispersion interactions, covalent bonds, and hydrogen bonding. For all four molecules under investigation, the values of adsorption energy were determined, thereby supporting the efficacy of CHA in removing these species. Moreover, the quantum chemistry calculations indicate that the introduction of Al into the zeolite structure can enhance the adsorption of polar species. Such an enhanced adsorption is attributed to the charge localization of HOMO orbitals. It is found that the HOMO of CHA displays delocalization across the entire Si-O framework, whereas the HOMO of CHA-Al_2 exhibits localization. This localized charge distribution is anticipated to result in more potent electrostatic or Van der Waals interactions with the adsorbents.

In contrast to the weak adsorption of dibutyl disulfide in the zeolite experiment, quantum chemistry revealed a high energy of adsorption observed for this species in interaction with the sorbent. We hypothesized that this is likely due to the linear shape of the molecule, which allows it to pass through the monolith channels without having sufficient time for interaction. Nevertheless, a more comprehensive study involving molecular dynamics is required for further investigation.

CRediT authorship contribution statement

Ehsan Alborzi: Writing – review & editing, Writing – original draft, Resources, Project administration, Methodology, Investigation, Funding acquisition, Formal analysis, Conceptualization. **Xue Yong:** Writing – review & editing, Investigation, Conceptualization. **Morteza Roostaeinia:** Investigation. **Detlev C. Mielczarek:** Writing – review & editing, Writing – original draft. **Irina S. Flyagina:** Writing – review & editing, Writing – original draft, Investigation. **Simon G. Blakey:** Writing – review & editing, Funding acquisition. **Mohamed Pourkashanian:** Writing – review & editing, Project administration.

Declaration of competing interest

The authors declare that they have no known competing financial interests or personal relationships that could have appeared to influence the work reported in this paper.

Data availability

Supplementary data will be made available.

Acknowledgments

This work was supported by the Horizon 2020-Clean Sky 2 programme under research grant agreement 150089. The authors acknowledge the University of Sheffield high performance computing services (Stanage and Bessemer clusters). Xue Yong is thankful to the financial support provided by Leverhulme trust.

References

[1] Hazlett RN. Thermal oxidation stability of aviation turbine fuels. ASTM; 1991.
[2] Taylor WF. Deposit formation from deoxygenated hydrocarbons. II. Effect of trace sulfur compounds. Ind Eng Chem Product Res Dev 1976-03;15(1):64–8. http://dx.doi.org/10.1021/i360057a012, URL http://pubs.acs.org/cgi-bin/doilookup/?10.1021/i360057a012.
[3] Taylor WF, Frankenfeld JW. Deposit formation from deoxygenated hydrocarbons. III. Effects of trace nitrogen and oxygen compounds. Ind Eng Chem Product Res Dev 1978;17(1):86–90. http://dx.doi.org/10.1021/i360065a021.
[4] Taylor S. An alternative view of the thermal oxidative stability of jet fuels. ACS Div Petroleum Chem Inc Preprints 2002;47(3):165–9.
[5] Boss D, Hazlett RN, Shepard RL. Analysis of n-Paraffin oxidation products in the presence of hydroperoxides. Anal Chem 1973;45(14):14–8.
[6] Zabarnick S. Pseudo-detailed chemical kinetic modeling of antioxidant chemistry for jet fuel applications. Energy Fuels 1998;12(3):547–53. http://dx.doi.org/10.1021/ef970157l.
[7] Zabarnick S, Mick MS. Inhibition of jet fuel oxidation by addition of hydroperoxide-decomposing species. Ind Eng Chem Res 1999;38(9):3557–63. http://dx.doi.org/10.1021/ie990107z.
[8] Zabarnick S, Phelps DK. Density functional theory calculations of the energetics and kinetics of jet fuel autoxidation reactions. Energy Fuels 2006;20(2):488–97. http://dx.doi.org/10.1021/ef050348l.
[9] Kuprowicz NJ, Ervin JS, Zabarnick S. Modeling the liquid-phase oxidation of hydrocarbons over a range of temperatures and dissolved oxygen concentrations with pseudo-detailed chemical kinetics. Fuel 2004;83(13):1795–801. http://dx.doi.org/10.1016/j.fuel.2004.03.013, URL http://linkinghub.elsevier.com/retrieve/pii/S0016236104001103.
[10] Kuprowicz NJ, Zabarnick S, West ZJ, Ervin JS. Use of measured species class concentrations with chemical kinetic modeling for the prediction of autoxidation and deposition of jet fuels. Energy Fuels 2007;21(2):530–44. http://dx.doi.org/10.1021/ef060391o.
[11] Denisov ET, Denisova T. Handbook of antioxidants: Bond dissociation energies, rate constants, activation energies, and enthalpies of reactions. 2nd ed. CRC Press; 1999.
[12] Denisov ET, Afanas'ev IB. Oxidation and antioxidants in organic chemistry and biology. CRC Press; 2005.
[13] Spadaccini L, Huang H. On-line fuel deoxygenation for coke suppression. J Eng Gas Turbines Power 2003;125(3):686–92. http://dx.doi.org/10.1115/1.1582497.
[14] Alborzi E, Gadsby P, Ismail MS, Sheikhansari A, Dwyer MR, Meijer AJHM, et al. Comparative study of the effect of fuel deoxygenation and polar species removal on jet fuel surface deposition. Energy Fuels 2019;33(3):1825–36. http://dx.doi.org/10.1021/acs.energyfuels.8b03468.
[15] Alborzi E, Parks CM, Gadsby P, Sheikhansari A, Blakey SG, Pourkashanian M. Effect of reactive sulfur removal by activated carbon on aviation fuel thermal stability. Energy Fuels 2020;34(6):6780–90. http://dx.doi.org/10.1021/acs.energyfuels.9b04370.
[16] Darrah S. Jet fuel deoxygenation, AFWAL-TR-88-2081 Interim Report,. Tech. rep. Air Force Wright Aeronautical Laboratory; Wright-Patterson AFB; OH); 1988.
[17] Van Bekkum H, Flanigen EM, Jensen JC. Introduction to zeolite and science practice. Elsevier; 1991.
[18] Jha B, Singh DN. Basics of zeolites. In: Fly ash zeolites. Advanced structured materials. Elsevier Inc.; 2016.
[19] Bendoraitis JG, Chester AW, Dwyer FG, Garwood WE. Pore size and shape effects in zeolite catalysis. Stud Surf Sci Catal 1986;28:669–75. http://dx.doi.org/10.1016/S0167-2991(09)60933-2.
[20] Alborzi E, Flyagina IS, Mielczarek DC, Blakey SG, Pourkashanian M. A theoretical investigation into the comparative adsorption between dissolved oxygen and oxygenate species on zeolite 3.7 åduring aviation fuel treatment for thermal stability improvement. Fuel 2022;317:123451. http://dx.doi.org/10.1016/j.fuel.2022.123451, URL https://www.sciencedirect.com/science/article/pii/S0016236122003167.
[21] Yang C-T, Janda A, Bell AT, Lin L-C. Atomistic investigations of the effects of Si/Al ratio and al distribution on the adsorption selectivity of n-alkanes in brønsted-acid zeolites. J Phys Chem C 2018;122(17):9397–410. http://dx.doi.org/10.1021/acs.jpcc.7b11190.
[22] Lohse U, Parlitz B, Patzelova V. Y zeolite acidity dependence on the silicon/aluminum ratio. J Phys Chem 1989;93(9):3677–83. http://dx.doi.org/10.1021/j100346a061.
[23] Simon-Masseron A, Marques J, Lopes J, Ribeiro FR, Gener I, Guisnet M. Influence of the Si/Al ratio and crystal size on the acidity and activity of HBEA zeolites. Appl Catal A General 2007;316(1):75–82. http://dx.doi.org/10.1016/j.apcata.2006.09.022, URL https://www.sciencedirect.com/science/article/pii/S0926860X06006843.
[24] Venkatesha NJ, Bhat YS, Jai Prakash BS. Dealuminated BEA zeolite for selective synthesis of five-membered cyclic acetal from glycerol under ambient conditions. RSC Adv 2016;6:18824–33. http://dx.doi.org/10.1039/C6RA01437B, URL http://dx.doi.org/10.1039/C6RA01437B.

[25] Mortier WJ, Bosmans HJ. Location of univalent cations in synthetic zeolites of the Y and X type with varying silicon to aluminum ratio. I. Hydrated potassium exchanged forms. J Phys Chem 1971;75(21):3327–34. http://dx.doi.org/10.1021/j100690a022.

[26] Katada N, Niwa M. Analysis of acidic properties of zeolitic and non-zeolitic solid acid catalysts using temperature-programmed desorption of ammonia. Catal Surv Asia 2004;8(3):161–70. http://dx.doi.org/10.1023/B:CATS.0000038534.37849.16.

[27] Suzuki K, Noda T, Katada N, Niwa M. IRMS-TPD of ammonia: Direct and individual measurement of brønsted acidity in zeolites and its relationship with the catalytic cracking activity. J Catal 2007;250:151–60.

[28] Munthali MW, Elsheikh MA, Johan E, Matsue N. Proton adsorption selectivity of zeolites in aqueous media: Effect of Si/Al ratio of zeolites. Molecules 2014;19(12):20468–81. http://dx.doi.org/10.3390/molecules191220468, URL https://www.mdpi.com/1420-3049/19/12/20468.

[29] Llorca J. Monolithic reactor. In: Drioli E, Giorno L, editors. Encyclopedia of membranes. Berlin, Heidelberg: Springer Berlin Heidelberg; 2015, p. 1–3. http://dx.doi.org/10.1007/978-3-642-40872-4_2203-1.

[30] VandeVondele J, Krack M, Mohamed F, Parrinello M, Chassaing T, Hutter J. Quickstep: Fast and accurate density functional calculations using a mixed Gaussian and plane waves approach. Comput Phys Comm 2005;167(2):103–28. http://dx.doi.org/10.1016/j.cpc.2004.12.014, URL https://www.sciencedirect.com/science/article/pii/S0010465505000615.

[31] Fletcher R. Practical methods of optimization. Wiley; 2013, URL https://books.google.fr/books?id=_WuAvIx0EE4C.

[32] Perdew JP, Burke K, Ernzerhof M. Generalized gradient approximation made simple. Phys Rev Lett 1996;77:3865–8. http://dx.doi.org/10.1103/PhysRevLett.77.3865, URL https://link.aps.org/doi/10.1103/PhysRevLett.77.3865.

[33] Goedecker S, Teter M, Hutter J. Separable dual-space Gaussian pseudopotentials. Phys Rev B 1996;54:1703–10. http://dx.doi.org/10.1103/PhysRevB.54.1703, URL https://link.aps.org/doi/10.1103/PhysRevB.54.1703.

[34] VandeVondele J, Hutter J. Gaussian basis sets for accurate calculations on molecular systems in gas and condensed phases. J Chem Phys 2007;127(11):114105. http://dx.doi.org/10.1063/1.2770708.

[35] Handbook of aviation fuel properties. 4th ed. Coordinating Research Council; 2014.

[36] Zabarnick S. Chemical kinetic modeling of jet fuel autoxidation and antioxidant chemistry. Ind Eng Chem Res 1993;32:1012–7.

[37] Zabarnick S, Grinstead RR. Studies of jet fuel additives using the quartz crystal microbalance and pressure monitoring at 140°C. Ind Eng Chem Res 1994;33:2771–7. http://dx.doi.org/10.1021/ie00035a029, URL http://www.scopus.com/inward/record.url?eid=2-s2.0-0028539598&partnerID=40&md5=7cdaa498ef67a75af71c1846e05d6224.

[38] Alborzi E, Dwyer MR, Parks CM, Sheikhansari A, Mielczarek DC, Zanganeh M, et al. Construction of a reduced chemical kinetic mechanism for autoxidation of n-paraffinic solvent – A model for aviation fuel. Fuel 2021;294:120170. http://dx.doi.org/10.1016/j.fuel.2021.120170, URL https://www.sciencedirect.com/science/article/pii/S0016236121000466.

[39] Bateman L, Hughes H, Morris A. Hydroperoxide decomposition in relation to the initiation of radical chain reactions. Discuss. Faraday Soc. 1953;14:190–9. http://dx.doi.org/10.1039/DF9531400190.

[40] Database of Zeolite Structures, https://europe.iza-structure.org/IZA-SC/material_tm.php?STC=CHA.